

# Erosion–Corrosion Behavior of 20Cr Steel in Corrosive Solid–Liquid Two-Phase Flow Conditions

Lu Cui  · Zhen Li · Yihua Dou

Submitted: 27 January 2018/in revised form: 22 February 2018/Published online: 9 April 2018  
© ASM International 2018

**Abstract** An experimental study was conducted on erosion–corrosion (E–C) properties of 20Cr (Chinese steel grade) steel. Three corrosive solid–liquid two-phase aqueous solutions (distilled water, 3.5 wt.% NaCl aqueous solutions and saturated CO<sub>2</sub> aqueous solutions, respectively, mixed with quartz grain) are used at three different experiments. The research confirmed that the E–C rate increased exponentially with the increase in flow velocity. The equation  $V_e = KV^n$  can be used to express the relationship between E–C rate and flow velocity. Furthermore, a new regression approach called ‘segment fitting’ was proposed. It had better fitting precision to express the relationship between E–C rate and flow velocity. The analysis and SEM surface topography show that the material removal rate is controlled by electrochemical corrosion at lower flow velocity and may suffer from mechanically induced deterioration at higher flow velocity. The impact angle has complex effects on E–C rate. In the experiment condition, the E–C rate will reach highest at 45° impact angle.

**Keywords** Low-alloy steel · Erosion–corrosion · Solid–liquid two-phase · Erosion–corrosion rate

## Introduction

In the marine, oil and gas production and power-generating industries, components are usually attacked by solid–liquid two-phase flow which causes E–C. Sometimes, the fluid is corrosive. It is important for the engineers to specify the relationship between flow velocities and E–C rate, to identify the main factors which affect the E–C rate in components, to reveal the E–C mechanism, to predict E–C rates in actual working circumstance or simply to try to convince engineers that corrosion can be a matter of concern when high flow velocities of corrosive solid–liquid two-phase flow are involved [1]. During the recent decades, researches for many aspects of flow-induced corrosion in all kinds of equipment such as oil and gas well tubulars, heat exchangers, pumps, hydraulic machines, steam generators, components for nuclear power stations and chemical plant have been carried out [2–5]. The research contents cover mechanisms, damage morphology and the affecting factors of E–C [6–9].

The E–C in downhole tubulars and oilfield ground gathering transferring system is one of the very serious problems in oil and gas production. The fluid usually contains carbon dioxide, chloride ions, dissolved oxygen and sometimes associates with sand. However, according to API specification 5CT [10], immersion tests or electrochemical corrosion tests in a beaker or a chamber were still the standard test procedure in the laboratory for materials selection. The effect of the flowing fluid on the tubulars is generally ignored in previous studies. During oil and gas production, loss of wall thickness and even puncture due to E–C is one of the main sources of failure of downhole tubulars. Photographs in Fig. 1 show the damage morphologies of the downhole tubulars due to E–C.

---

L. Cui · Z. Li · Y. Dou (✉)  
School of Mechanical Engineering, Xi’an Shiyou University,  
Xi’an 710065, Shaanxi, China  
e-mail: yhdou@vip.sina.com

L. Cui  
e-mail: cuiluxa@hotmail.com



**Fig. 1** Macro-damage morphology of downhole tubular outer surface caused by erosion–corrosion

**Table 1** Chemical composition of testing material 20Cr (wt.%)

C	Si	Mn	Cr	S	P	Ni
0.19	0.26	0.59	0.89	0.0046	0.0020	0.021

So it is very necessary to investigate the E–C properties of oil tubulars under oil and gas production environment, where carbon dioxide, chloride ions and dissolved oxygen associate with sand are to be taken into consideration. In this article, typical material of 20Cr for oilfield ground gathering transferring system is selected. The relationship between E–C rate and flow velocity is experimentally studied. The effect of the flow impact angle on the E–C rate is investigated through experiments. And then, the morphology of specimen surface is analyzed by SEM after testing.

**Experimental Method**

**Material and Specimen Preparation**

The material used for experiments is a low-carbon low-alloy steel 20Cr (Chinese steel grade, compatible to AISI 5120) used for oilfield ground gathering transferring system. The chemical composition and mechanical properties are shown in Tables 1 and 2 separately.

The specimens were machined into cylinder with a 10 mm in diameter and a 15 mm in height. The upper surface of each specimen was wet ground with SiC paper up to the 2000 grit. The bottom and side surfaces were protected by epoxy resin during the experiment, as shown in Fig. 2. The specimen was washed by using absolute alcohol and dried below 50 °C.

**Table 2** Mechanical properties of testing material 20Cr

Tensile strength $\sigma_b$ (MPa)	0.2% yield strength $\sigma_s$ (MPa)	Elongation $\delta$ (%)	Reduction of cross section $\psi$ (%)
883.7	652.6	18.5	50.8

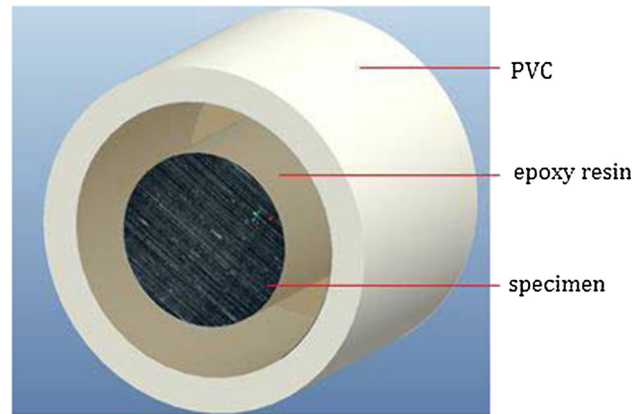


**Fig. 2** Geometry of erosion–corrosion specimen

**Fluid Preparation**

Three aqueous solutions were used as the E–C media. Each kind of fluid (distilled water, 3.5 wt.% NaCl aqueous solutions and saturated CO<sub>2</sub> aqueous solutions) was mixed with quartz grain with 210–420 μm in diameter. All the fluids were prepared in laboratory environment. To clarify, saturated CO<sub>2</sub> aqueous solution was obtained through injecting CO<sub>2</sub> into distilled water continuously during experiment.

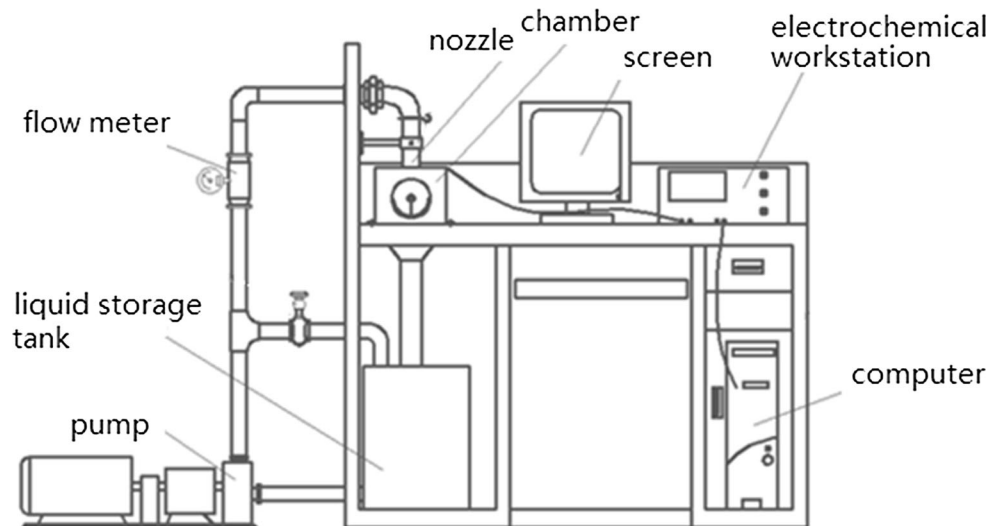
**Experiment Equipment**

The E–C experiments were carried out in a jet impingement experimental apparatus, as shown in Fig. 3. It consists of a large stainless steel tank (30 cm in length, 30 cm in width and 40 cm in height) from which the prepared fluid with quartz grain is drawn using a calibrated pump. The flow rate of the liquid was controlled by a bypass line and was measured by a magnetic flow meter. BSA5201 analytical balance is used to measure weight precisely. Its accuracy is 0.1 mg. E–C morphology of specimen surface was observed by means of JSM-6390 scanning electron microscopy.

**Experiment Procedure**

First of all, net weight of the original specimen without protecting material was measured. After the preparation work mentioned in “[Material and Specimen Preparation](#)”

**Fig. 3** Jet impingement experimental equipment



section, the specimen with protecting material was fixed in a holder. The impact angle was adjusted through setup of the angle between specimen surface and the axes of nozzle. Then, the experiment could be started by turning on the calibrated pump. The appropriate fluid velocity was guaranteed by adjusting frequency converter. After a given period testing, stop the calibrated pump, remove the specimen from the holder, separate the specimen from protecting material and clean it. Re-measure the weight of the specimen. The weight loss of specimen can be obtained:

$$\Delta W = W_0 - W_1 \quad (\text{Eq 1})$$

where  $\Delta W$  is the weight loss of specimen in gram,  $W_0$  is the initial weight of the specimen,  $W_1$  is the weight of the specimen suffering from corrosion test after removal of corrosion products. The E–C rate is formulated as follows:

$$V_e = \frac{\Delta W}{\rho \cdot A \cdot t} \times 10^3 \times 60 \times 24 \times 365 = \frac{5.256 \times 10^8 \Delta W}{\rho \cdot A \cdot t} \quad (\text{Eq 2})$$

where  $V_e$  is the E–C rate in mm/a,  $A$  is the specimen surface area exposed to corrosive environment,  $t$  is testing time, and  $\rho$  is the density of tested metal in g/cm<sup>3</sup>.

### Experimental Results and Analysis

The effect of flow velocity on the E–C rate was carried out by a constant flow impact angle of 45° (Fig. 4a). It was observed that the changing trends of E–C rate versus flow velocity in the tested three media were similar. E–C rate of this material in the mentioned three media increased slowly with the increase in flow velocity until the flow velocity

reaches around 15 m/s. After that, the E–C rate increased rapidly.

The influence of flow velocity on E–C rate can be described as the following equation [12]:

$$V_e = AV_p^n F(\alpha) \quad (\text{Eq 3})$$

where  $V_e$  is the E–C rate.  $V_p$  is the impact velocity of the sand particle on the metal surface.  $A$  and  $n$  are experimentally determined constants that depend on the material properties. For ductile materials the value of  $n$  is in the range of 2–3. For brittle material,  $n$  can be as high as 6.  $F(\alpha)$  is a function whose value varies between 0 and 1, depending on the impact angle  $\alpha$  [12]. The determination of sand particle impact angle,  $\alpha$ , and impact velocity,  $V_p$ , is difficult, because they may not be the same as the total amount of sand in the flow. It is difficult to obtain the E–C rate  $V_e$  through Eq 3. For a certain experiment condition of constant flow velocity,  $V_p$  can be replaced with the flow velocity  $V$ . Moreover, when the specimen is held at a fixed angle, regard  $F(\alpha)$  as a constant. So Eq 3 can be changed to:

$$V_e = KV^n \quad (\text{Eq 4})$$

where  $K$  is experimentally determined constant.

In order to analyze the effect flow velocity on E–C rate, the regression analysis was made for experimental results by using Eq 4. The fitting curves are shown in Fig. 4a. The parameters  $K$  and  $n$  in Eq 4 for the three media and the correlation coefficient  $r$  are shown in Table 3.

The effect of impact angle on E–C rate is shown in Fig. 4b for example at a flow velocity of 10 m/s. The E–C rate increases with the increase in impact angle firstly and decreases with a maximum E–C rate at impact angle of 45°. Generally, the E–C rate at smaller impact angle is larger than that at higher impact angle.

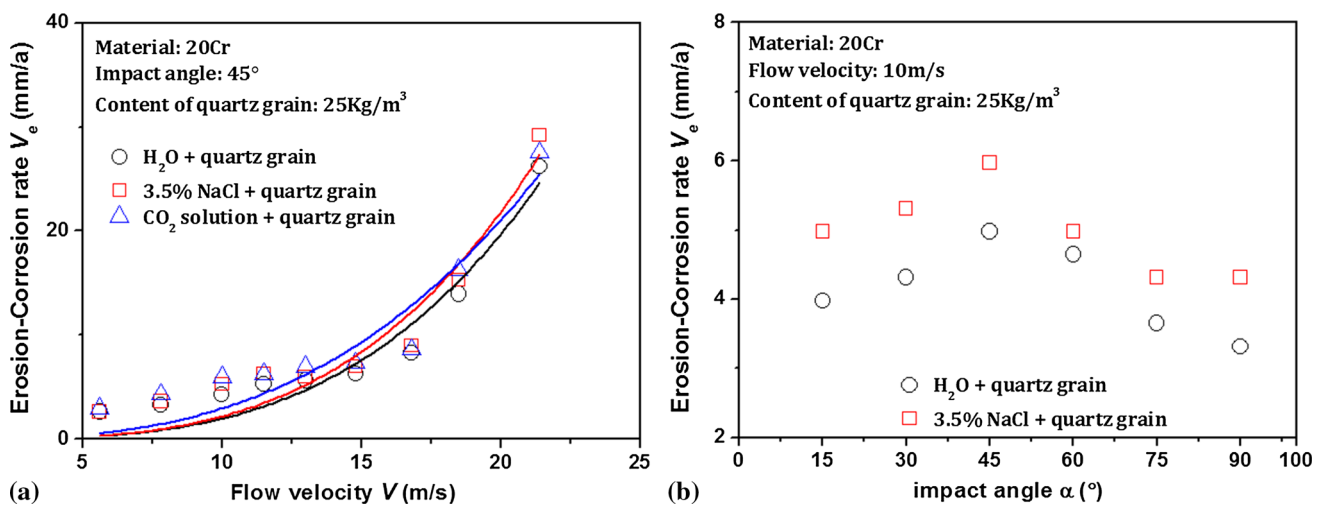


**Fig. 4** Relation between flow velocity and E–C rate by a flow impact angle of 45° (a) and relation between flow impact angle  $\alpha$  and E–C rate by a flow velocity of 10 m/s (b)

**Table 3** Parameters  $K$  and  $n$  in Eq 4 for the three media

	$K(-)$	$n(-)$	Correlation coefficient $r(-)$
H2O + quartz grain	$9.86 \times 10^{-4}$	3.30544	0.90977
3.5% NaCl + quartz grain	$1.06 \times 10^{-3}$	3.31556	0.89819
CO2 solution + quartz grain	$4.44 \times 10^{-3}$	2.82486	0.87382

**Discussion**

The Effect of Flow Velocity on E–C Rate

E–C occurs when solid particles suspended in the slurry impact the surface of the material. The synergistic interaction between the electrochemical reactions and mechanical forces applied by solid particles causes damage much more than the sum of individual damages caused by each of these phenomena. However, the mechanism of synergistic interaction is very complex. It depends on the corrosive fluid, target material, passive film, shape and mechanical properties of solid particles, velocity and direction of fluid and solid particles impact to target material, and so on [13, 14]. Although many formulas have been put forward [15], it is difficult to use them in the prediction of E–C rate for a certain working condition. Therefore, there is no common conclusion about E–C rate expression. As shown in Fig. 4a, the precision of nonlinear regression analysis using Eq. 4 is relatively low. In the three media, the correlation coefficient between E–C rate and flow velocity is only 0.90977, 0.89819 and 0.87382, respectively.

Nesic’s work [16] pointed out that E–C occurs at very high flow velocities when the entrained solids cause erosion of protective layers and can even lead to damage of the underlying steel. As the relationship of E–C rate and medium flow velocity is presented in double logarithm coordinate, it is very clear that E–C rate grows linearly during the increase in the flow velocity. The E–C rate gradient is significantly different at low flow velocity and at high velocity (Fig. 5). In the low flow velocity area, E–C rate in the flow of saturated CO<sub>2</sub> aqueous solutions mixed with quartz grain is greater than that in the flow of 3.5 wt.% NaCl and distilled water mixed with quartz grain. However, when it is subjected to higher flow velocity, there are no significant differences in E–C rate among the tested results. The corrosion damage is dominant at low flow velocity, while the wear-out effect of solid particles on metal surface is dominant at high flow velocity. Therefore, the slope of E–C rate changes at the critical flow velocity. Because of differences in corrosion resistance of material among three media, the differences of E–C rate at lower flow velocity among them were significant. One can infer that the material removal rate is mainly controlled by electrochemical corrosion, and the erosion by solid particles is the secondary cause. At higher flow velocity, E–C rate in three media is nearly the same because of the same experiment conditions except for corrosive substance. It may suffer from mechanically induced deterioration. However, the relatively low flow rates and the lack of flow disturbances in pipelines rarely give rise to E–C problems.

The characterization of surface topography is analyzed through scanning electron microscopy (SEM) as shown in Fig. 6. These are also the evidence for the conclusion mentioned above. When the hard particles were added to the corrosive solution, the mechanism model for E–C by

which material is removed from the target surface was proposed in the literature of Levy and Crook [17] and López et al. [18]. A possible sequence of events could account for the improvement in E–C resistance of the studied surfaces: pores, small cracks and fresh pits can be covered by the prows and lips that are formed as a consequence of the wedge action of round particles (Fig. 7). SEM images show some evidences of the mechanism model for E–C. Figure 6a–c shows the surface texture suffering from the flow of 3.5 wt.% NaCl mixed with quartz grain at a flow velocity of 7.8, 13.0 and 21.4 m/s, respectively, by a flow impact angle of 45°. The results show that the number of pits caused by solid particles goes up while flow velocity is increased. In Fig. 6a, b, there are still some areas, in which material surface was not impacted by solid particles. Corrosion caused by corrosive substance occurs in these areas. In Fig. 6c, the material surface is completely covered by impact pits. It suffers from mechanically induced deterioration.

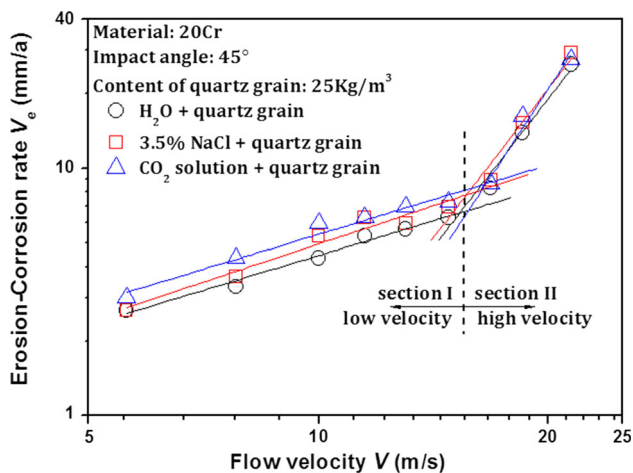


**Fig. 5** Experimental results and ‘segment fitting’ curve of relations between flow velocity and E–C rate

According to the E–C damage mechanism mentioned above, a new regression approach called ‘segment fitting’ is proposed. Equation 5 is derived by logarithming on both sides of Eq. 4.

$$\log V_e = \log K + n \log V \quad (\text{Eq 5})$$

The experimental results are plotted in logarithmic scales in Fig. 5. As mentioned above, relation of E–C rate and flow velocity is divided into two sections, lower velocity and higher velocity. In both sections, E–C rate grows linearly as the flow velocity increases in the double logarithm coordinate. The parameters  $K$  and  $n$  and the correlation coefficient  $r$  for three media by ‘segment fitting’ are determined as shown in Table 4. ‘Segment fitting’ results and experimental results are plotted in Fig. 5. They are in good agreement with the test results.

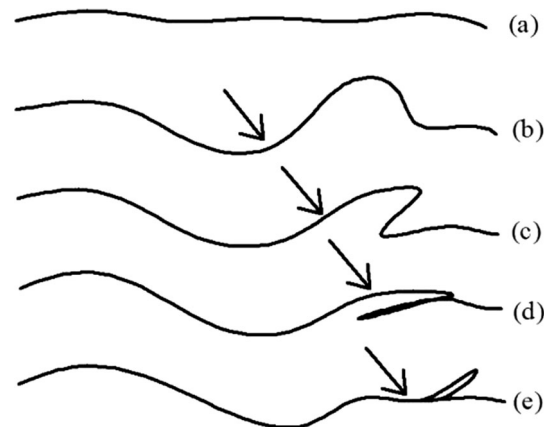


**Fig. 7** Simplified model to explain the beneficial effect of plastic deformation caused by hard particles on E–C resistance of ductile surfaces. (a) Surface previous to the first impact, (b) a particle impacts the surface and forms prows and lips, (c) a pit initiates due to corrosive attack, (d) successive particle impacts shift material over the pit, (e) highly deformed material closes the pit, thin flake debris was peeled off, or some internal cracks remain [17, 18]

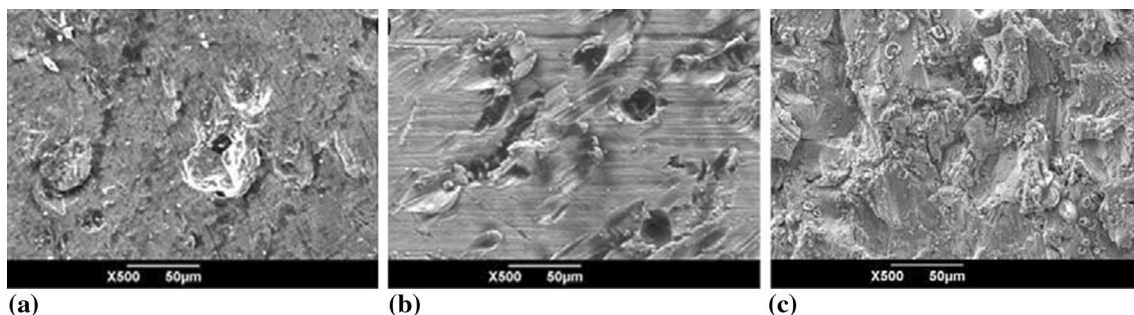


**Fig. 6** Surface topography suffering from the flow of 3.5 wt.% NaCl mixed with quartz grain at a flow velocity of 7.8 m/s (a), 13.0 m/s (b) and 21.4 m/s (c)

**Table 4** Parameters  $K$  and  $n$  of ‘segment fitting’ for the three media

	Section I: at lower velocity			Section II: at higher velocity		
	$K(-)$	$n(-)$	Correlation coefficient $r(-)$	$K(-)$	$n(-)$	Correlation coefficient $r(-)$
H2O + quartz grain	0.52	0.93074	0.98336	$1.27 \times 10^{-4}$	3.97969	0.96197
3.5% NaCl + quartz grain	0.47	1.02165	0.95025	$1.27 \times 10^{-4}$	4.01136	0.95327
CO2 solution + quartz grain	0.63	0.93305	0.97245	$1.602 \times 10^{-5}$	4.70147	0.9428

The Effect of Impact Angle on E–C Rate

As shown in Fig. 4b, the experimental results indicate that the E–C rate at lower impact angle is larger than that at higher impact angle, and reached highest at 45° impact angle. The experimental results are coincided with the conclusions of related studies. Previous studies show that the impact angle has complex effects on E–C rate. For brittle material, E–C rate will increase monotonically with the increase in the impact angle of the fluid, and E–C rate will reach highest at 90° impact angle [19]. For ductile material, the conclusions from different studies are inconsistent. Burstein and Sasaki studied the effect of the impact angle on the E–C of AISI 304L stainless steel and found that the maximum values of both erosion and E–C rates in chloride solution occurred at oblique angles between 40° and 50°, and that the synergism was positive in all conditions and greater for lower angles [18]. For 1017 steel in slurry, the erosion rate increases with the increase in the impingement angle up to a maximum value after which it decreases. The maximum erosion rate appears at 45° impingement angle [19]. On the other hand, it has been found that the maximum of erosion corrosion damage occurs at lower impact angles around 30° [20–22]. Also single impingement experiments have shown that the erosion enhanced corrosion becomes maximum at 30° impact angle [23].

Conclusions

The experimental measurements of E–C rate in three media of solid–liquid two-phase flow (distilled water, 3.5 wt.% NaCl aqueous solutions and saturated CO<sub>2</sub> aqueous solutions, respectively, mixed with quartz grain with 210–420 μm in diameter) were conducted to characterize the corrosion properties of 20Cr steel which is widely used in oilfield ground gathering transferring system. The relationship between E–C rate and flow velocity and the effect of impact angle on E–C rate were carried out. The experimental results revealed that the E–C rate increased exponentially with the increase in flow velocity. Furthermore, the experimental results could be divided into two parts, lower velocity and higher velocity section. Using

equation  $V_e = KV^n$  ‘segment fitting’ method has higher fitting precision. When it is subjected to lower flow velocity, E–C rate in the flow of saturated CO<sub>2</sub> aqueous solutions mixed with quartz grain was greater than it in the flow of 3.5 wt.% NaCl and distilled water mixed with quartz grain. However, when it is subjected to higher flow velocity, there were no significant differences in E–C rate. The SEM surface topography analysis showed that the material removal rate was controlled by electrochemical corrosion at lower flow velocity and may suffer from mechanically induced deterioration at higher flow velocity. The impact angle had complex effects on E–C rate. The E–C rate at lower impact angle was larger than that at higher impact angle and will reach highest at 45° impact angle.

**Acknowledgments** Thanks are due to the National Natural Science Foundation Program of China (No. 51305348) and Youth Pearl River Nova Program of Shaanxi (2015KJXX-37).

References

1. J. Werer, Flow induced corrosion: 25 years of industrial research. *Br. Corros. J.* **27**, 193–199 (1992)
2. X. Jiang, Y.G. Zheng, W. Ke, Effect of flow velocity and entrained sand on inhibition performances of two inhibitors for CO<sub>2</sub> corrosion of N80 steel in 3% NaCl solution. *Corros. Sci.* **47**, 2636–2658 (2005)
3. A. Neville, T. Hodgkiess, An assessment of the corrosion behaviour of high-grade alloys in seawater at elevated temperature and under a high velocity impinging flow. *Corros. Sci.* **38**, 927–956 (1996)
4. E.A.M. Hussain, M.J. Robinson, Erosion–corrosion of 2205 duplex stainless steel in flowing seawater containing sand particles. *Corros. Sci.* **49**, 1737–1754 (2007)
5. S.H. Shah, S. Jain et al., Coiled tubing erosion during hydraulic fracturing slurry flow, in *SPE Conference*, Houston, 2004
6. Y. Yang, Y.F. Cheng, Parametric effects on the erosion–corrosion rate and mechanism of carbon steel pipes in oil sands slurry. *Wear* **276–277**, 141–148 (2012)
7. K.S. Tan, J.A. Wharton, R.J.K. Wood, Solid particle erosion–corrosion behaviour of a novel HVOF nickel aluminum bronze coating for marine applications—correlation between mass loss and electrochemical measurements. *Wear* **258**, 629–640 (2005)
8. A. Neville, M. Reyes et al., Mechanisms of wear on a Co-base alloy in liquid–solid slurries. *Wear* **238**, 138–150 (2000)
9. B.T. Lu, L.C. Mao, J.L. Luo, Hydrodynamic effects on erosion-enhanced corrosion of stainless steel in aqueous slurries. *Electrochim. Acta* **56**, 87–90 (2010)
10. API, *API Specification 5CT, Specification for Casing and Tubing*, 9th edn. (American Petroleum Institute, Washington, DC, 2011)

11. H-j Zhu, Y-h Lin, D-z Zeng, R-t Yan, Simulations of flow induced corrosion in API drillpipe connector. *J. Hydrodyn.* **23**(6), 784–791 (2011)
12. M.M. Salama, An alternative to API 14E erosional velocity limits for sand-laden fluids. *J. Energy Resour. Technol.* **122**, 71–77 (2000)
13. F. Mohammadi, J. Luo, Effects of particle angular velocity and friction force on erosion enhanced corrosion of 304 stainless steel. *Corros. Sci.* **52**, 2994–3001 (2010)
14. R.J.K. Wood, Erosion–corrosion interactions and their effect on marine and offshore materials. *Wear* **261**, 1012–1023 (2006)
15. S.S. Rajahram, T.J. Harvey, R.J.K. Wood, Evaluation of a semi-empirical model in predicting erosion–corrosion. *Wear* **267**, 1883–1893 (2009)
16. S. Nestic, Effects of multiphase flow on internal CO<sub>2</sub> corrosion of mild steel pipelines. *Energy Fuels* **26**, 4098–4111 (2012)
17. A.V. Levy, P. Crook, The erosion properties of alloys for the chemical processing industries. *Wear* **151**, 337–350 (1991)
18. D. López et al., Effect of particle velocity and impact angle on the corrosion-erosion of AISI 304 and AISI 420 stainless steels. *Wear* **259**, 118–124 (2005)
19. M.A. Al-Bukhaiti et al., Effect of impingement angle on slurry erosion behaviour and mechanisms of 1017 steel and high-chromium white cast iron. *Wear* **262**, 1187–1198 (2007)
20. G.T. Burstein, K. Sasaki, Detecting electrochemical transients generated by erosion corrosion. *Electrochim. Acta* **46**, 3675–3683 (2001)
21. M. Matsumura, Y. Oka, H. Hiura, M. Yano, The role of passivating film in preventing slurry erosion corrosion of austenitic stainless steel. *ISIJ Int.* **31**, 168–176 (1991)
22. X. Tanga, L.Y. Xua, Y.F. Cheng, Electrochemical corrosion behavior of X-65 steel in the simulated oil sand slurry. II: synergism of erosion and corrosion. *Corros. Sci.* **50**, 1469–1474 (2008)
23. A.J. Smitha, M. Stratmann, A.W. Hassel, Investigation of the effect of impingement angle on tribocorrosion using single impacts. *Electrochim. Acta* **51**, 6521–6526 (2006)